U.S. DEPARTMENT OF ENERGY | Office of Science

DOE/SC-CM-24-002

FY 2024 Second Quarter Performance Metric: Demonstrating and Evaluating Kilometer-Scale Regional Refinement Modeling Capability in Simulated Water Cycle Extremes in the U.S.

Lai-Yung Ruby Leung
Paul Ullrich
Lead Authors

Xiaodong Chen
Jianfeng Li
Ning Sun
Sourav Taraphdar
Colin Zarzycki
Contributing Authors

April 2024

DISCLAIMER

Contents

Figures

1.0 Product Definition

Increasing the horizontal grid resolution in atmosphere models has been shown to lead generally to improvements in modeling extreme events such as extreme precipitation produced by thunderstorms (e.g., Pope and Stratton 2002, Roekner et al. 2006, Wehner et al. 2010, Jong et al. 2023). At higher resolutions, atmosphere models can produce stronger vertical motions, for example, by better resolving the temperature and moisture gradients associated with fronts and tropical cyclones and representing the orographic uplift associated with mountains, and subsequently the higher condensation rates needed to generate intense precipitation associated with storms. However, atmosphere models simulate the precipitation processes using physics parameterizations such as cloud microphysics and convection with resolution- and time step-dependent behaviors, which complicate the relationship between model resolution and the simulated mean and extreme precipitation (e.g., Kopparla et al. 2013, Yang et al. 2014, Wehner et al. 2021).

Global kilometer-scale models that have emerged in the last decade (Stevens et al. 2019) hold great promise to further improve modeling of extreme weather events by explicitly resolving deep convection, a major mechanism for generating extreme precipitation, and potentially improving the simulation of mesoscale and large-scale atmospheric environments for the storms. Recently, the Energy Exascale Earth System Model (E3SM) project funded by the U.S. Department of Energy developed a global kilometer-scale model called Simple Cloud-Resolving E3SM Atmosphere Model (SCREAM) (Caldwell et al. 2021). Implementation of SCREAM, including innovative algorithmic and software engineering advancements to run on the Frontier Exascale computer, has demonstrated a groundbreaking performance of computational throughput > 1 simulated year per day (SYPD) (Taylor et al. 2023). However, running decadal-to-century-scale simulations using global kilometer-scale models remains computationally challenging, especially for quantifying the statistics of extreme events and their future changes (which typically requires large ensemble simulations). To circumvent such computational challenges, SCREAM has a regional refinement capability that allows kilometer-scale modeling to be performed in regions of interest within the context of global modeling at coarser resolutions outside those regions. This capability was first demonstrated in a study that used SCREAM with regional refinement over the central-eastern U.S. for simulating the strong winds and convection associated with a derecho event (Liu et al. 2023).

Building on the demonstration of Liu et al. (2023), this report documents the configurations and evaluation of SCREAM using regional refinement for kilometer-scale simulations of cold-season and warm-season storm events that produce extreme precipitation across diverse geographical regions in the U.S. Three examples are included to demonstrate the regional refinement capability of SCREAM to simulate (1) atmospheric rivers that made landfall in the U.S. Pacific Northwest Puget Sound basin that produced flooding, (2) mesoscale convective systems and isolated deep convection in the central-eastern U.S. that produced heavy precipitation in the region, and (3) a blizzard in the northeastern U.S. that produced snow and ice that damaged energy infrastructure. The results provide clear evidence that using regional refinement at 3.25-km grid spacing, the SCREAM model provides a scientifically robust and computationally efficient capability for simulating a variety of extreme weather events, including atmospheric rivers, mesoscale convective systems, and winter storms, across different geographies and regions of the contiguous U,S. Such capability is critical for understanding water cycle extremes such as

flooding caused by heavy precipitation, rain-on-snow events, and compound events, as well as ice storms that cause disruptions and power outages.

2.0 Product Documentation

This report documents the modeling of water cycle extremes in the U.S. using SCREAM with regional refinement capability for kilometer-scale modeling. This capability is demonstrated using three examples of simulating cold-season and warm-season storms in the U.S. underlined by different processes. SCREAM is configured for a global domain at 25-km grid spacing with regional refinement at 3.25-km grid spacing covering part of the U.S. and the surrounding ocean where the storms developed. As SCREAM does not include any parameterization of deep convection, which is needed at 25-km grid spacing, nudging was applied to constrain the SCREAM simulations with the European Center for Medium-Range Forecast Reanalysis version 5 (ERA5) (Hersbach et al. 2020) outside the refined region. Initialized using atmospheric conditions from ERA5, the simulations, each covering 5-50 days, were compared with observations to demonstrate the model skill in simulating important water cycle aspects of the storm events.

2.1 Landfalling Atmospheric Rivers in the Puget Sound Basin

Atmospheric rivers (ARs) are narrow bands of intense atmospheric moisture transport across the subtropics (Zhu and Newell 1998). ARs often produce heavy precipitation and strong winds and induce hazardous flooding when they make landfall over mountainous regions such as the west coast of the U.S., South America, and Europe (Leung and Qian 2009, Waliser and Guan 2017, Chen et al. 2019). On the other hand, ARs provide critical snowpack water storage for the western U.S., which depends strongly on snowpack for water supply during dry summer months (Dettinger et al. 2011). SCREAM was used to simulate five ARs that made landfall and led to major flooding in the Puget Sound basin of the U.S. Pacific Northwest between 2006 and 2022. These five AR cases also represent different ground snowpack conditions at the time of AR landfall, allowing evaluation of SCREAM in modeling the interplay between AR landfall and snowpack conditions, and their consequential impact on flooding. This report summarizes the simulations for the first AR case to compare two versions of SCREAM (Donahue et al. in review) and the results from all five AR cases that used the newer version that produced more skillful results. The refined region (Figure 1) was configured to match the domain of the Weather Research and Forecasting (WRF) regional model configured at 3-km grid spacing and driven by ERA5 lateral boundary conditions for comparison.

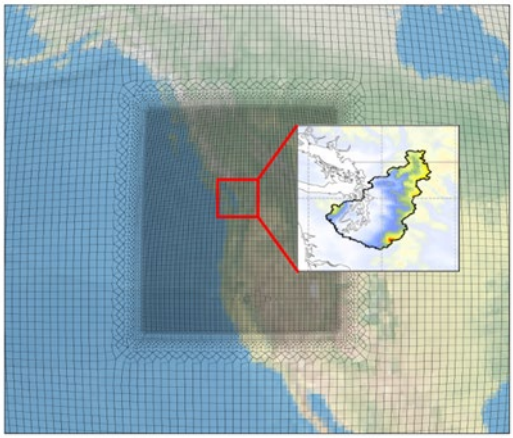

Figure 1. The SCREAM domain featuring a refined region at 3.25-km grid spacing over the U.S. Pacific Northwest and the northeastern Pacific Ocean within a global domain at 25-km grid spacing. Nudging was applied to grid cells outside the transition zone with grid spacing varying from 3.25 km to 25 km. The Puget Sound basin, lying between the Olympic Mountains to its west and the Cascade Range to its east, is shown in the inset and demarcated by the black boundary.

2.2 Convective Storms in the Central Eastern U.S.

Frequent convective storms that occur in the central-eastern US during the warm season provide water to support agriculture in the region, but large mesoscale convective systems (MCSs) and intense isolated deep convection (IDC) can produce slow-rising and flash floods and strong winds with significant societal and economic consequences (Hu et al. 2021). SCREAM was configured to simulate the populations of MCS and IDC during a 50-day period of July 1-August 19, 2020, with the model initialized on June 28, 2020 using HRRR (James et al. 2020) and ERA5. Nudging was applied outside the refined region to constrain the 25-km simulation with ERA5. The MCSs and IDC in the simulation and observation were tracked using an updated Flexible Object Tracker (FLEXTRKR; Feng et al. 2019) algorithm described in Li et al. (2021) for evaluation of the statistics and properties of MCSs and IDC simulated by SCREAM.

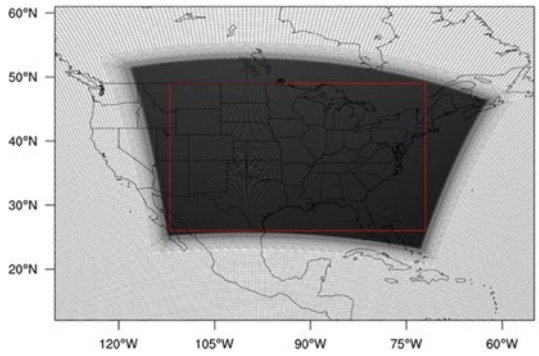

Figure 2. The SCREAM domain featuring regional refinement over the central-eastern U.S. at 3.25-km grid spacing within a global domain of 25-km grid spacing. Nudging was applied to all grid cells outside the red box.

2.3 A Blizzard in the Northeastern U.S.

The northeastern U.S. is frequently subject to extreme winter storms that bring heavy snowfall with subsequent impacts on infrastructure and travel (Zielinski 2002). These storms are usually driven by intense low-pressure systems that propagate eastwards, drawing warm moist air from the Gulf of Mexico and the Atlantic coast that is subject to uplift and cooling along associated cold frontal bands. The recent 2016 North American Blizzard, also known as Winter Storm Jonas and Snowzilla, occurred during January 23-24, 2016 and was estimated to have affected over 100 million people (Halverson 2016). Seven states observed snow accumulations over 30 inches, and at least 55 people were killed in storm-related incidents. Economic losses were estimated to be over one billion dollars. To simulate this storm, SCREAM was employed at 3-km grid spacing over the central-eastern U.S. (Figure 3). The focus of this report is on the ability of SCREAM to simulate snowfall amounts and timing.

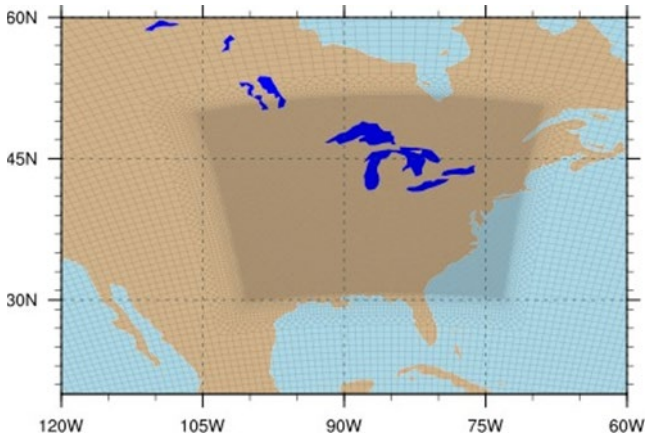

Figure 3. The SCREAM domain for the 2016 North American Blizzard simulation, featuring regional refinement over the central-eastern U.S. at 3.25-km grid spacing within a global domain of 25-km grid spacing.

3.0 Results

3.1 Landfalling Atmospheric Rivers in the Puget Sound Basin

SCREAM was configured to simulate five AR events, each featuring different ground snowpack characteristics, that led to regional floods. These events include heavy rain without pre-existing snowpack (November 2006), a mix of rain and snow resulting in snow accumulation (January 2009), rain-on-snow (January 2011), antecedent snow drought (February 2015), and compound flooding caused by the AR-induced rain-on-snow, storm surge, and a concurrent king tide in the coastal region (December 2022) (Figure 4). The SCREAM simulations were compared with observations and the WRF simulations configured at 3-km grid spacing for the same region as the SCREAM refined domain. WRF was used to produce an ensemble of 10 simulations using different combinations of atmospheric physics parameterizations, two land surface models, and two reanalysis boundary conditions (ERA5 and the North American Regional Reanalysis [NARR]).

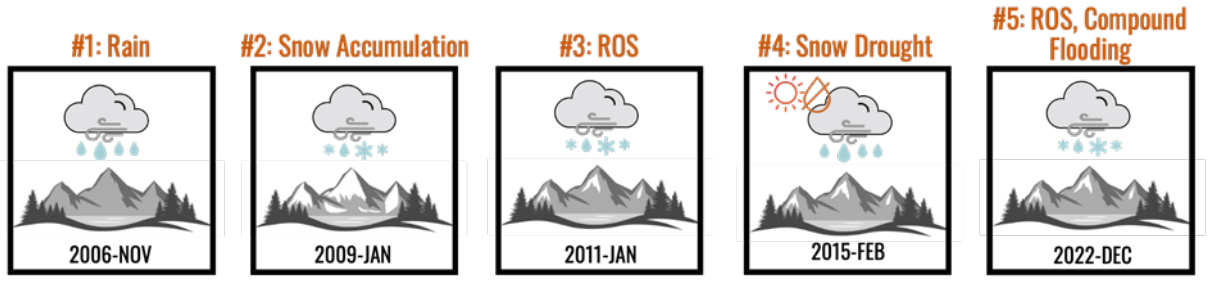

Figure 4. A schematic summarizing the key features of five atmospheric river events that made landfall in the Puget Sound basin between 2006 and 2020. The runoff response to ARs is generally amplified in rain-on-snow (ROS) events (#3 and #5) while ARs that predominantly produce rainfall (#1) versus snowfall (#2) differ in the timing of the runoff response. The antecedent snow drought condition (#4) precludes ROS and limits the runoff response to AR.

As the first case study among the five AR cases, the November 2006 AR was simulated using two versions of SCREAM. The older version (Caldwell et al. 2021) was used to participate in the DYAMOND (The DYnamics of the Atmospheric general circulation Modeled On Non-hydrostatic Domains) global cloud-resolving model intercomparison for the boreal winter simulation (Stevens et al. 2019). More recently, changes have been made to SCREAM to address some known issues such as the frequent appearance of 'popcorn'-like convection and precipitation objects. For example, the new version sets ice cloud fraction based on cell-average ice mass mixing ratio, while the old version used a relative humidity-based ice cloud fraction (Donahue et al. in review). Here the two versions of SCREAM are referred to as "Old-SCREAM" and "New-SCREAM", respectively. Figure 5 compares the integrated vapor transport (IVT), precipitable water (PW), winds at 850 hPa, and precipitation in observations and the two SCREAM simulations averaged over November 1-10, 2006. Improvements in simulating all the quantities are noticeable in New-SCREAM compared to Old-SCREAM. With orographic forcing from the Coastal Range and the Cascade Range, two north-south oriented bands of heavy precipitation are prominently noted in the observation. While the Old-SCREAM simulation produced a heavy precipitation band along the Coastal Range, precipitation is much weaker over the Cascade Range where the Puget Sound basin is located. In contrast, the New-SCREAM simulation produced two heavy precipitation bands comparable to those observed, although with weaker magnitude. The improvements in the New-SCREAM precipitation are consistent with the more eastward- and inland-penetrating IVT, PW, and winds that brought more moisture to the Cascade Range compared to Old-SCREAM. Such changes in atmospheric circulation are attributed to changes in the diabatic heating, with the New-SCREAM producing stronger diabatic heating than Old-SCREAM along the Cascade Range (Figure 6). The stronger middle-upper-level heating produced stronger middle-level vorticity that increased the lower-level convergence through Ekman pumping and increased instability and precipitation in the Cascade Range. The difference in diabatic heating between the two SCREAM simulations is related to recent changes made to the cloud microphysics parameterization that produced much lower ice number concentration and slightly higher ice and liquid mass mixing ratios. These changes increased the diabatic heating in the middle troposphere that increased the lower-level moisture convergence as noted earlier.

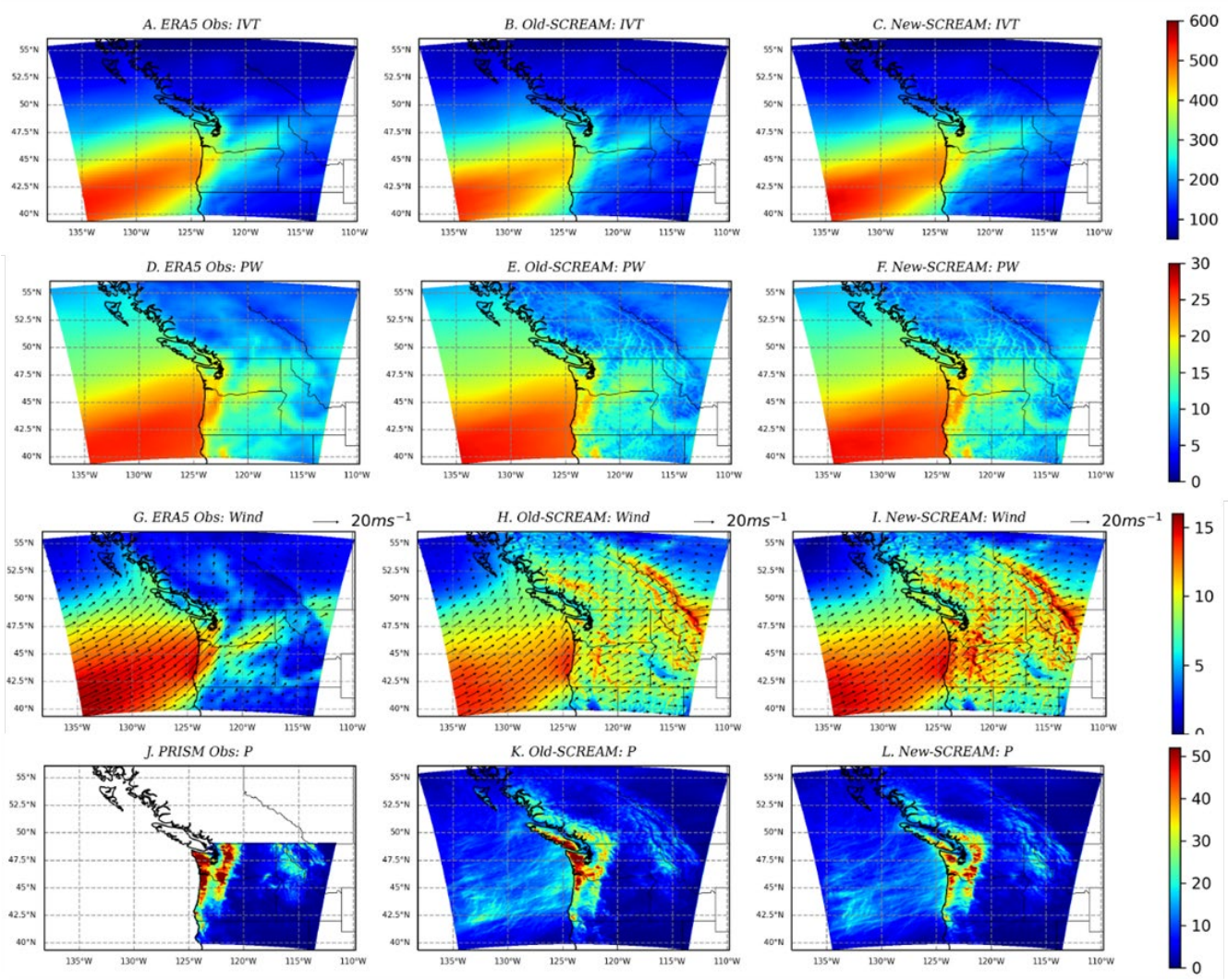

Figure 5. Spatial distributions of integrated vapor transport (IVT, kg m^{-1} s^{-1})) (A-C), precipitable water (PW, mm) (D-F), wind (m s^{-1}) (G-I) and precipitation (mm day^{-1}) (J-L) in observations (left), Old-SCREAM (middle), and New-SCREAM (right). Observations for IVT, PW, and wind are based on ERA5 and observations for precipitation are based on the PRISM data at 4-km grid spacing.

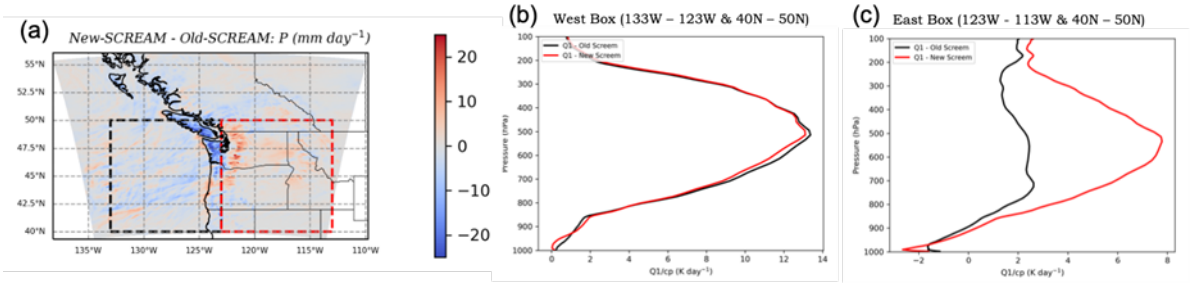

Figure 6. (a) Spatial distribution of the difference in precipitation (mm day-1) between New-SCREAM and Old-SCREAM. Diabatic heating (K day-1) averaged over the west box (b) and east box (c) simulated by Old-SCREAM (black) and New-SCREAM (red). The west and east boxes are shown in panel (a).

As similar improvements from the New-SCREAM were consistently found in other AR cases, this version, referred simply as SCREAM hereafter, was used to simulate all five ARs that made landfall in the Puget Sound basin (Figure 7). For all five ARs, SCREAM realistically simulated the Puget Sound basin average precipitation and surface temperature compared to observations. Notably, the SCREAM simulations generally resemble the ensemble mean of the 10 WRF simulations in all cases. Using different physics and lateral boundary conditions, the WRF ensemble simulations produced a range of precipitation and temperature that generally enveloped the observed time series. During AR events, heavy precipitation typically occurred during periods with above freezing temperature, which contributed to flooding induced by heavy rainfall and/or rain-on-snow (ROS) process. Both ROS events (January 2011 and December 2022) were well simulated by SCREAM for precipitation amount and temperature, which are both important for simulating the runoff response.

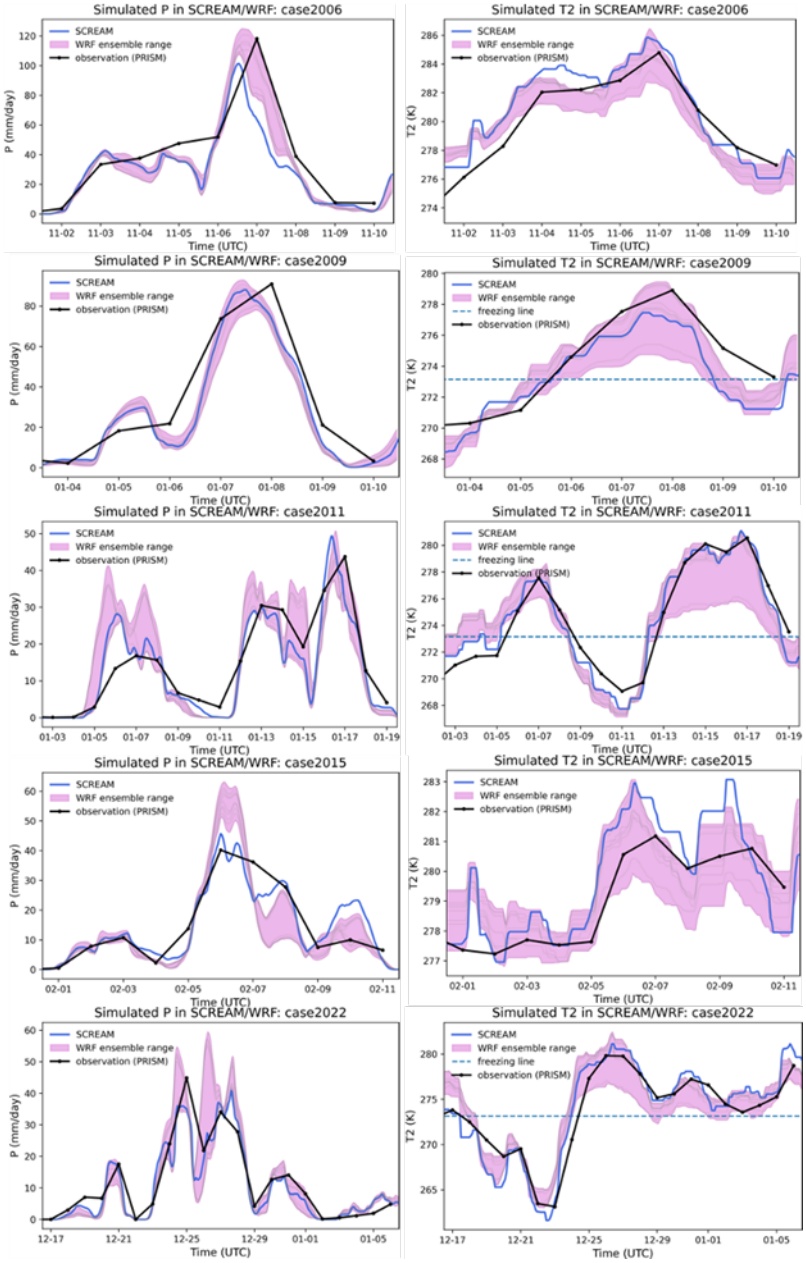

Figure 7. Time series of observed (black), SCREAM simulated (blue), and WRF simulated (thin light blue) Puget Sound basin mean precipitation (left) and surface temperature (right) for five ARs that made landfall in the Puget Sound basin between 2006 and 2020. Each of the 10 ensemble members of WRF simulations is shown in thin light blue with the pink shaded area showing the range of values represented by the ensemble simulations. From top to bottom are the 5 AR cases corresponding to cases #1 to #5 in Figure 3. The horizontal dashed blue line indicates the freezing temperature. Each simulation covered 10 to 20 days before, during, and after the ARs made landfall.

To illustrate how errors in simulating precipitation and temperature translate to biases in modeling streamflow, the SCREAM and WRF simulated temperature and precipitation were used as input to the Distributed Hydrology Soil Vegetation Model (DHSVM) (Wigmosta and Lettenmaier 1999) applied at 150-m grid spacing over the Puget Sound basin. Figure 8 compares the observed and simulated streamflow at a stream gauge in a subbasin of the Puget Sound for the December 2022 compound flooding AR case. The peak precipitation and temperature biases in SCREAM are -10% and 0.16 K respectively, and for WRF, these biases range from -7% to 33% and -1 K to 1.25 K with an ensemble mean of -11% and 0.41 K. The observed streamflow during the AR event was generally well captured by DHSVM driven by the SCREAM and WRF input. For the peak streamflow that occurred on 28 December, 2022, the DHSVM simulation driven by SCREAM and the ensemble mean of the DHSVM simulations driven by WRF both showed a bias of 27%. Contrasting the 27% bias in streamflow with the -10% and -11% precipitation biases in SCREAM and the WRF ensemble mean suggests important contributions of ROS to the runoff during this AR event.

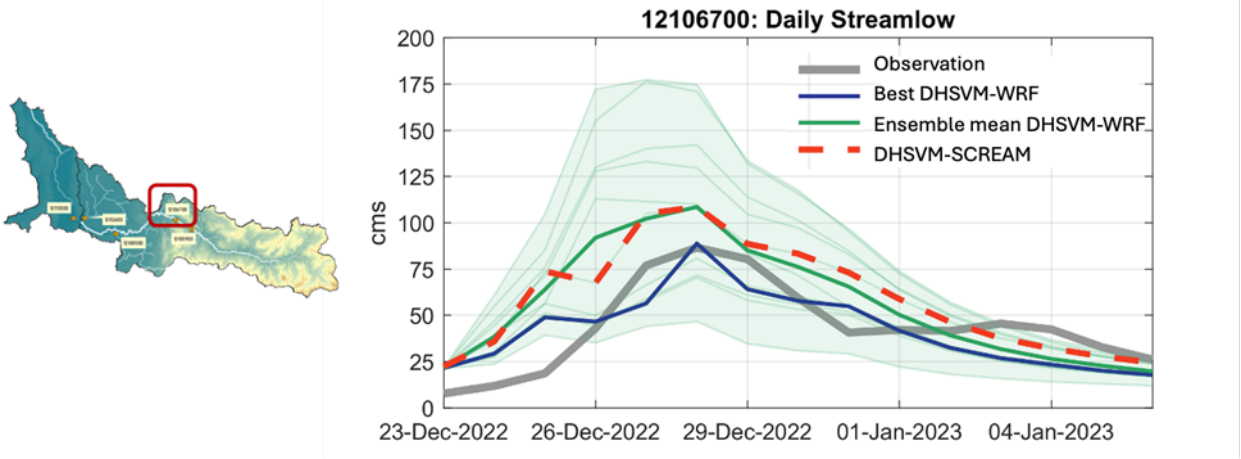

Figure 8. Observed (thick grey line) and DHSVM simulated daily streamflow at a stream gauge location shown on the left within the Puget Sound basin for the December 2022 atmospheric river event. The DHSVM simulations include those driven by the SCREAM simulation (dashed red line) and an ensemble of WRF simulations (light green shaded area), with the ensemble mean DHSVM simulation shown in green and the WRF-driven DHSVM simulation that best matches the observed streamflow shown in blue.

3.2 Convective Storms in the Central-Eastern U.S.

Climate models at grid spacings of 25-100 km struggle to simulate mesoscale convective systems (MCSs) and isolated deep convection (IDC) due to limitations of the deep convection parameterizations (Lin et al. 2017, Feng et al. 2021). In the refined region at 3.25-km grid spacing without any parameterizations of deep convection, SCREAM skillfully reproduced many statistics and characteristics

of MCS and IDC during the 50 days (July 1-August 19, 2020) compared to the MCS-IDC data set produced by Li et al. (2021) based on observations. As summarized in Table 1, SCREAM simulated 66 MCSs with an averaged lifetime of 18.4 h and convective and stratiform rain rates of 4.6 mm h^{-1} and 2.6 mm h^{-1}, which are comparable to the 80 MCSs tracked in observations with an averaged lifetime of 18.6 h and convective and stratiform rain rates of 4.6 mm h^{-1} and 2.8 mm h^{-1}. The MCSs in SCREAM also display similar spatial structures such as cold cloud systems (CCS) area and CCS major axis length as the MCSs found in observations, but the simulated precipitation feature (PF) convective and stratiform areas are noticeably larger than those observed. Contrary to MCS, SCREAM simulated too many IDC events (19,638) compared to observations (15,887), but similar to MCS, SCREAM also simulated larger PF convective and stratiform areas compared to observations. Overall, the large contrast between the MCS and IDC statistics and properties (size, lifetime, etc.) is well simulated by SCREAM at 3.25-km grid spacing.

Table 1. Comparison of the SCREAM simulated MCS and IDC statistics and mean properties in the U.S. east of the Rocky Mountains with an observational MCS-IDC data set. Cold cloud systems (CCS) are continuous areas with brightness temperature (Tb) < 241 K and CCS cores are areas with Tb < 225 K, indicating areas with deep convection. Precipitation feature (PF) areas are defined as continuous areas with smoothed radar reflectivity at 2 km > 28 dBZ. Intense convective cells are identified by maximum reflectivity exceeding 40 dBZ.

Convection Statistics and Properties	MCS		IDC	
	Obs	SCREAM	Obs	SCREAM
Event number (#)	80	66	15,887	19,638
Lifetime (h)	18.6	18.4	1.8	1.5
CCS area (km^2)	127,560	116,552	2,970	2,927
CCS core area (km^2)	66,444	55,516	667	647
Max 40-dBZ echo top height (km)	9.2	6.9	5.4	5.0
PF convective area (km^2)	8,363	12,911	388	970
PF stratiform area (km^2)	22,405	27,325	558	777
PF convective rain rate (mm h^{-1})	4.6	4.1	4.3	3.7
PF stratiform rain rate (mm h^{-1})	2.8	2.6	2.9	2.2
CCS major axis length (km)	524	515	67	75
PF major axis length (km)	297	323	47	59
Convective core major axis length (km)	122	114	26	42

East of the Rocky Mountains, MCSs produced heavy precipitation in the Great Plains, with the maximum accumulated precipitation reaching 350 mm during the 50 days (Fig. 9a). SCREAM generally reproduced the spatial distribution of MCS precipitation showing larger amounts in the Great Plains, although regional differences compared to the observations, such as an eastward shift in MCS precipitation, are also apparent (Fig. 9c). Instead of the Great Plains, IDC precipitation is mostly found in southeastern U.S., especially along the Gulf Coast, Florida, and the lower East Coast (Fig. 9b). This spatial distribution of IDC is quite well simulated by SCREAM except in the lower East Coast where the SCREAM IDC precipitation is much weaker (Fig. 9d).

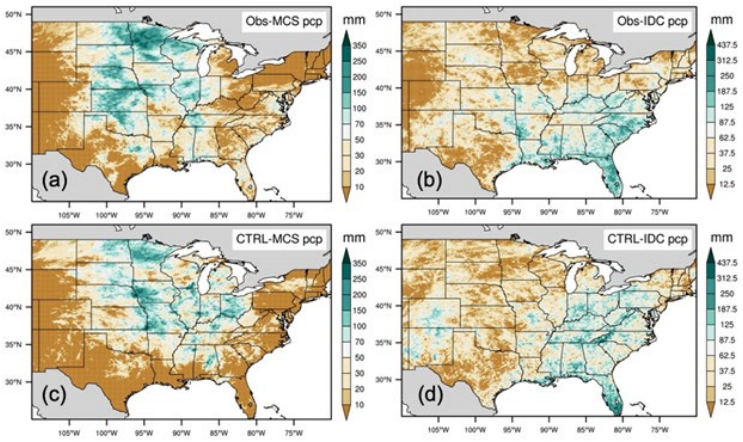

Figure 9. Spatial distributions of accumulated precipitation produced by MCS and IDC in the SCREAM simulation and observations during July 1-August 19, 2020.

To evaluate the variations in the MCS properties simulated by SCREAM throughout the MCS life cycle, Figure 10 displays the composited evolution of MCS properties as a function of its lifetime normalized to 20 h. After MCS initiation at 0 h, the MCS CCS grows in size to reach a maximum at ~10 h after which the CCS area shrinks until the MCS dissipates at 20 h. Consistent with the results summarized in Table 1, the CCS area is well simulated by SCREAM (Fig. 10a), although the CCS core area corresponding to the deep convective core with brightness temperature < 225 K tends to be smaller (Figure 10b), and the convection strength as depicted by the maximum 40-dBZ echo top height is weaker than observed (Figure 10c). Opposite to the CCS, the SCREAM PF areas for both convective and stratiform precipitation area are larger than observed (Figure 10d, e). Consistent with the weaker convection as indicated by the convection strength, the SCREAM MCSs produce weaker convective and stratiform rain rates during the growth period of the MCS (Figure 10f, g). Both the CCS and PF major axis lengths are very well simulated by SCREAM, suggesting realistic spatial structure of the squall line in the model (Figure 10h, i).

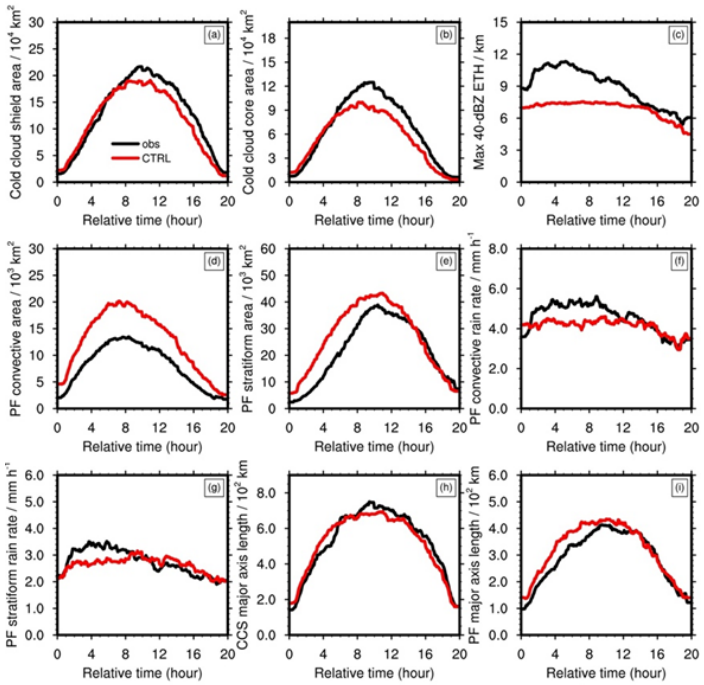

Figure 10. Normalized and composited evolutions of MCS properties from the observational MCS-IDC dataset and the SCREAM simulation east of the Rocky Mountains for July 1-August 19, 2020.

3.3 A Blizzard in the Northeastern U.S.

To simulate the 2016 North American Blizzard, SCREAM is initialized on January 21, 2016 at 0Z using initial conditions interpolated from ERA5 and run until January 26, 2016 at 0Z. Model initialization and spin-up was conducted using the Betacast framework (Zarzycki and Jablonowski 2015). Validation in this report focuses on SCREAM's ability to simulate the spatial distribution and magnitude of snow during an extreme winter storm. Snowfall from high-impact winter storm systems can be difficult for climate models to simulate because it is the result of a complicated series of processes from large-scale dynamics through sub-grid-scale microphysics. For comparison, we use the daily 4km University of Arizona gridded snow water equivalent (UofA SWE) from assimilated in-situ and modeled data (Broxton et al., 2019). Accumulated SWE, averaged over each day of the storm, is depicted in Figure 11. Relative to UofA SWE, SCREAM does an excellent job at simulating the pattern of the SWE, but at its peak, is about 30% greater in magnitude. However, because of deficiencies in the observing network and difficulties in capturing ephemeral snowpack, uncertainties in the magnitude of SWE in the eastern U.S. are likely large (Broxton et al. 2016), and so we are careful not to attribute all of SCREAM's overestimate in SWE to model bias. To support this claim, we plot the SCREAM simulated snow depth alongside Global Historical Climatology Network (GHCN; Peterson et al. 1998) observed snow depth at three stations along the storm trajectory in Figure 12. Results show that SCREAM correctly captures the timing of the storm and performs reasonably well at estimating the snow depth in each location, tending to slightly overestimate snow depth to the southwest and overestimate to the northeast.

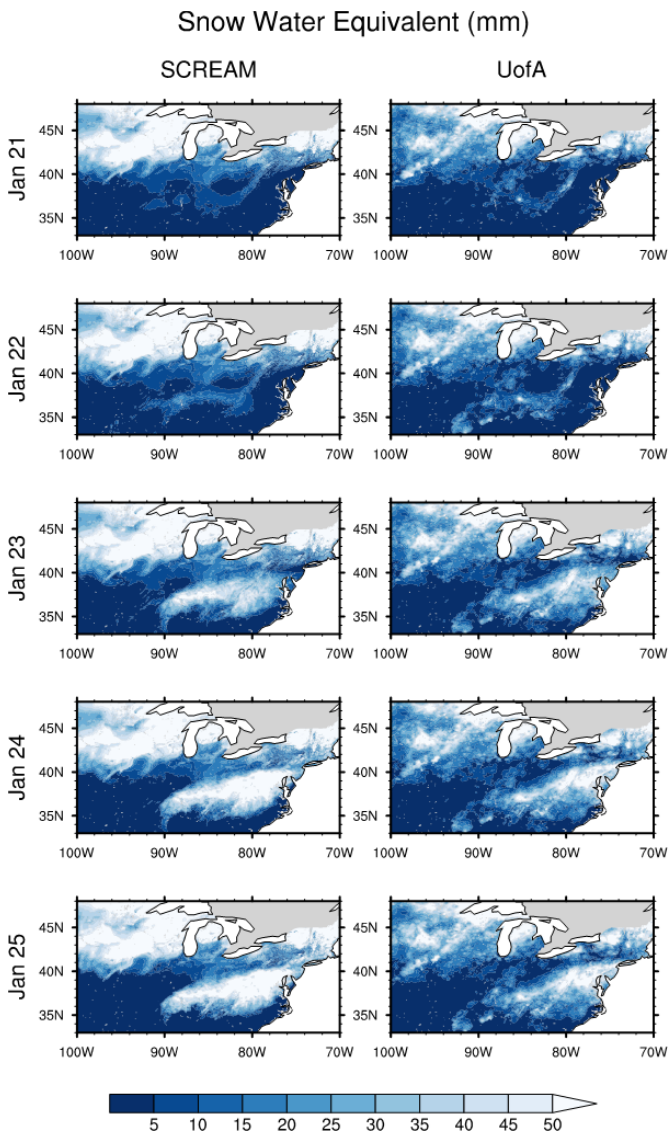

Figure 11. Average daily snow water equivalent (SWE) over the northeastern contiguous U.S., as obtained from (left column) the SCREAM simulation and (right column) the UofA gridded snow product for the period January 21-26, 2016.

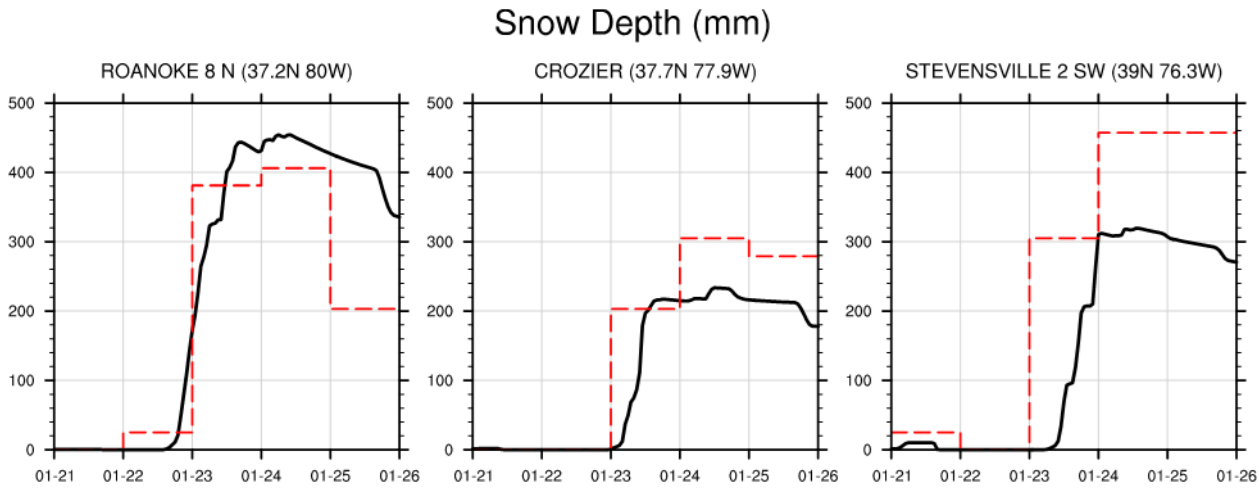

Figure 12. Snow depth in (mm) at three GHCN observing stations in the eastern U.S., roughly oriented from southwest to northeast. In each case, SCREAM modeled snow depth is depicted with the black line while daily GHCN observations are depicted with the red dashed line.

4.0 Summary and Future Work

The results highlighted in this report provide clear evidence that, using regional refinement, the SCREAM model demonstrates both computationally efficiency and a robust capability to simulate a variety of extreme weather events, including atmospheric rivers, mesoscale convective systems, and winter storms. These events include a variety of geographies and regions, with broad coverage of the contiguous United States. To demonstrate the efficacy of the model for simulating these features, several relevant process-oriented and impacts-relevant metrics and diagnostics have been evaluated. The relatively strong performance of SCREAM and its robustness across a variety of metrics and features suggests that it is a powerful tool for addressing scientific inquiries related to these features. Discrepancies between the model and observations should not be misconstrued as evidence of model deficiency, as they are also influenced by factors such as atmospheric variability and uncertainties in the initial conditions and observational networks. Overall, DOE has made dramatic progress in the development of a robust cloud-system resolving modeling capability for global and regional simulations, and the results of this report are evidence of the latter and their utility to the scientific community.

Notably, simulations of the type considered here are commonly employed in storyline-type simulations, which pair a historical simulation with a future analog to explore how high-impact events may change under global warming (Shepherd 2019). While regional models have been used exclusively in previous works for storyline simulations (e.g., Xue et al. 2023, Feng et al. 2024), the SCREAM regionally refined model is highly amenable to be used in the generation of future analog events. It provides a complementary and potentially more powerful approach for storyline simulations by overcoming some limitations of regional models associated with the formulation of the lateral boundary conditions. SCREAM storyline simulations are planned for many of the features described in this paper under modified environmental conditions.

5.0 References

Broxton, PD, X Zeng, and N Dawson. 2016. "Why do global reanalyses and land data assimilation products underestimate snow water equivalent?" *Journal of Hydrometeorology* 17(11): 2743–2761, https://doi.org/10.1175/JHM-D-16-0056.1

Broxton, P, X Zeng, and N Dawson. 2019. Daily 4 km Gridded SWE and Snow Depth from Assimilated In-Situ and Modeled Data over the Conterminous U.S., Version 1 (Data Set). Boulder, Colorado USA. NASA National Snow and Ice Data Center Distributed Active Archive Center. https://doi.org/10.5067/0GGPB220EX6A. Accessed 03-07-2024.

Caldwell, PM, CR Terai, B Hillman, ND Keen, P Bogenschutz, W Lin, H Beydoun, M Taylor, L Bertagna, AM Bradley, TC Clevenger, AS Donahue, C Eldred, J Foucar, J-C Golaz, O Guba, R Jacob, J Johnson, J Krishna, W Liu, K Pressel, AG Salinger, B Singh, A Steyer, P Ullrich, D Wu, X Yuan, J Shpund, H-Y Ma, and CS Zender. 2021. "Convection-permitting simulations with the E3SM global atmosphere model." *Journal of Advances in Modeling Earth Systems* 13(11): e2021MS002544, https://doi.org/10.1029/2021MS002544

Chen, X, LR Leung, M Wigmosta, and M Richmond. 2019. "Impact of atmospheric rivers on surface hydrological processes in western U.S. watersheds." *Journal of Geophysical Research – Atmospheres* 124(16): 8896–8916, https://doi.org/10.1029/2019JD030468

Dettinger, MD, FM Ralph, T Das, PJ Neiman, and DR Cayan. 2011. "Atmospheric rivers, floods and the water resources of California." *Water* 3(2): 445–478, https://doi.org/10.3390/w3020445

Donahue, AS, PM Caldwell, L Bertagna, H Beydoun, PA Bogenshutz, A Bradley, TC Clevenger, JG Fourcar, J-C Golaz, O Guba, WM Hannah, BR Hillman, J Johnson, ND Keen, W Lin, B Singh, MA Taylor, J Tian, CR Terai, P Ullrich, X Yuan, and Y Zhang. 2024. "To exascale and beyond – The Simple Cloud-Resolving E3SM Atmosphere Model (SCREAM), a performance portable global atmosphere model for cloud-resolving scales." *Journal of Advances in Modeling Earth Systems*, in review.

Feng, Z, F Song, K Sakaguchi, and LR Leung. 2021. "Evaluation of mesoscale convective systems in climate simulations: methodological development and results from MPAS-CAM over the U.S." *Journal of Climate* 34(7): 2611–2633, https://doi.org/10.1175/JCLI-D-20-0136.1

Feng, Z, X Chen, and LR Leung. 2024. "How might the May 2015 flood in the U.S. Southern Great Plains induced by clustered MCSs unfold in the future?" *Journal of Geophysical Research – Atmospheres*, accepted.

Halverson, JB. 2016. "The East Coast Blizzard of 2016: The Northeast Gets Buried." *Weatherwise* 69(4): 12–17, https://doi.org/10.1080/00431672.2016.1182846

Hersbach, H, B Bell, P Berrisford, S Hirahara, A Horányi,J Muñoz-Sabater, J Nicolas, C Peubey, R Radu, D Schepers, A Simmons, C Soci, S Abdalla, X Abellan, G Balsamo, P Bechtold, G Biavati, J Bidlot, M Bonavita, G De Chiara, P Dahlgren, D Dee, M Diamantakis, R Dragani, J Flemming, R Forbes, M Fuentes, A Geer, L Haimberger, S Healy RJ Hogan, E Hólm, M Janisková, S Keeley, P Laloyaux, P Lopez, C Lupu, G Radnoti, P de Rosnay, I Rozum, F Vamborg, S Villaume, J-N Thépaut. 2020. "The ERA5 global reanalysis." *Quarterly Journal of the Royal Meteorological Society* 146(730): 1999–2049, https://doi.org/10.1002/qj.3803

Hu, H, Z Feng, and LR Leung. 2021. "Linking flood. frequency with mesoscale convective systems in the central U.S." *Geophysical Research Letters* 48(9): e2021GL092546, https://doi.org/10.1029/2021GL092546

James, EP, CR Alexander, DC Dowell, SS Weygandt, SG Benjamin, GS Manikin, JM Brown, JB Olson, M Hu, TG Smirnova, T Ladwig, JS Kenyon, and DD Turner. 2022. "The High-Resolution Rapid Refresh (HRRR): an hourly updating convection-allowing forecast model. Part II: Forecast performance." *Weather and Forecasting* 37(8): 1397–1417, https://doi.org/10.1175/WAF-D-21-0130.1

Jong, BT, TL Delworth, WF Cooke, KC Tseng, and H Murakami. 2023. "Increases in extreme precipitation over the Northeast United States using high-resolution climate model simulations." *npj Climate and Atmospheric Science* 6(1): 18, https://doi.org/10.1038/s41612-023-00347-w

Kopparla, P, EM Fischer, C Hannay, and R Knutti. 2013. "Improved simulation of extreme precipitation in a high- resolution atmosphere model." *Geophysical Research Letters* 40(21): 5803–5808, https://doi.org/10.1002/2013GL057866

Leung, LR, and Y Qian. 2009. "Atmospheric rivers induced heavy precipitation and flooding in the western U.S. simulated by the WRF regional climate model." *Geophysical Research Letters* 36(3): L03820, https://.doi.org/10.1029/2008GL036445

Li, J, Z Feng, Y Qian, and LR Leung. 2021. "A high-resolution unified observational database of mesoscale convective systems and isolated deep convection in the United States for 2004-2017." *Earth Syst. Science Data* 13(2): 827–856, https://doi.org/10.5194/essd-2020-151

Liu, W, PA Ullrich, J Li, C Zarzycki, PM Caldwell, LR Leung, and Y Qian. 2023. "The June 2012 North American derecho: A testbed for evaluating regional and global climate modeling systems at cloud-resolving scales." *Journal of Advances in Modeling Earth Systems* 15(4): e2022MS003358, https://doi.org/10.1029/2022MS003358

Peterson, TC, R Vose, R Schmoyer and V Razuvaëv. 1998. "Global Historical Climatology Network (GHCN) quality control of monthly temperature data." *International Journal of Climatology* 18(11): 1169–1179, https://doi.org/10.1002/(SICI)1097-0088(199809)18:11<1169::AID-JOC309>3.0.CO;2-U

Pope, V, and R Stratton. 2002. "The processes governing horizontal resolution sensitivity in a climate model." *Climate Dynamics* 19(3): 211–236, https://doi.org/10.1007/s00382-001-0222-8

Roeckner, E, R Brokopf, M Esch, M Giorgetta, S Hagemann, L Kornblueh, E Manzini, U Schlese, and U Schulzweida. 2006. "Sensitivity of simulated climate to horizontal and vertical resolution in the ECHAM5 atmosphere model." *Journal of Climate* 19(16): 3771–3791, https://doi.org/10.1175/JCLI3824.1

Shepherd, TG. 2019. "Storyline approach to the construction of regional climate change information." *Proceedings of the Royal Society A* 475(2225): 20190013, https://doi.org/10.1098/rspa.2019.0013

Stevens, B, M Satoh, L Auger, J Biercamp, CS Bretherton, X Chen, P Düben, F Judt, M Khairoutdinov, D Klocke, C Kodama, L Kornblueh, S-J Lin, P Neumann, WM Putnam, N Röber, R Shibuya, B Vanniere, PL Vidale, N Wedi, and L Zhou. 2019. "DYAMOND: the DYnamics of the Atmospheric general circulation Modeled On Non-hydrostatic Domains." *Progress in Earth and Planetary Science* 6(1): 1–17, https://doi.org/10.1186/s40645-019-0304-z

Taylor, MA, PM Caldwell, L Bertagna, C Clevenger, AS Donahue, JG Foucar, O Guba, BR Hillman, N Keen, J Krishna, MR Norman, S Sreepathi, CR Terai, JB White III, D Wu, AG Salinger, RB McCoy, LR Leung, DC Bader, and D Wu. 2023. "The Simple Cloud-Resolving E3SM Atmosphere Model running on the Frontier Exascale system." *SC'23: Proceedings of the International Conference for High Performance Computing, Networking, Storage and Analysis, November 2023, Article No.* 7:1–11, https://doi.org/10.1145/3581784.3627044

Waliser, D, and B Guan. 2017. "Extreme winds and precipitation during landfall of atmospheric rivers." *Nature Geoscience* 10(3): 179–183, https://doi.org/10.1038/ngeo2894

Wehner, M, J Lee, M Risser, P Ullrich, P Gleckler, and WD Collins. 2021. "Evaluation of extreme sub-daily precipitation in high-resolution global climate model simulations." *Philosophical Transactions of the Royal Society A*, 379(2195): 20190545, https://doi.org/10.1098/rsta.2019.0545

Wehner, M, R Smith, G Bala, and P Duffy. 2010. "The effect of horizontal resolution on simulation of very extreme U.S. precipitation events in a global atmosphere model." *Climate Dynamics* 34(2-3): 241–247, https://doi.org/10.1007/s00382-009-0656-y

Wigmosta, MS, and DP Lettenmaier. 1999. "A comparison of simplified methods for routing topographically driven subsurface flow." *Water Resources Research* 35(1): 255–264, https://doi.org/10.1029/1998WR900017

Xue, Z, PA Ullrich, and LR Leung. 2023. "Sensitivity of the pseudo-global warming method under flood conditions: a case study from the northeastern US.". *Hydrology and Earth System Sciences* 27(9): 1909–1927, https://doi.org/10.5194/hess-27-1909-2023

Yang, Q, LR Leung, S Rauscher, T Ringler, and M Taylor. 2014. "Spatial resolution dependence of precipitation extremes from atmospheric moisture budgets in aqua-planet simulations." *Journal of Climate* 27(10): 3565–3581, https://doi.org/10.1175/jcli-d-13-00468.1

Zarzycki, CM, and C Jablonowski. 2015. "Experimental tropical cyclone forecasts using a variable-resolution global model." *Monthly Weather Review* 143(10): 4012–4037, https://doi.org/10.1175/MWR-D-15-0159.1

Zielinski, GA. 2002. “A classification scheme for winter storms in the eastern and central United States with an emphasis on nor'easters.” *Bulletin of the American Meteorological Society* 83(1): 37–52, https://doi.org/10.1175/1520-0477(2002)083<0037:ACSFWS>2.3.CO;2

Zhu, Y, and RE Newell. 1998. “A proposed algorithm for moisture fluxes from atmospheric rivers.” *Monthly Weather Review* 126(3): 725–735, https://doi.org/10.1175/1520-0493(1998)126<0725:APAFMF>2.0.CO;2

U.S. DEPARTMENT OF
ENERGY

Office of Science